ELSEVIER

Journal of Fluids and Structures 25 (2009) 1189–1205

JOURNAL OF FLUIDS AND STRUCTURES

www.elsevier.com/locate/jfs

A numerical investigation of waves propagating in the spinal cord and subarachnoid space in the presence of a syrinx

C.D. Bertram

Biofluid Mechanics Laboratory, Faculty of Engineering, University of New South Wales, Sydney 2052, Australia

Received 8 January 2009; accepted 30 June 2009
Available online 15 August 2009

Abstract

The term syringomyelia describes fluid-filled cavities in the spinal cord, which can interfere with normal nerve signal transmission. The finite-element code ADINA was used to construct an axisymmetric fluid/structure-interaction model of the tapered spinal cord and subarachnoid space (SAS), bounded by the dura mater. A syrinx was simulated, of corresponding dimensions to one shown by magnetic resonance imaging data of a patient with syringomyelia. The model was used to investigate the clinical hypothesis that SAS pressure waves move fluid along a syrinx and can thus lengthen it over time by tissue dissection. Simplified versions of the model were used to examine in detail the waves excited, and their reflection and refraction at sites of property discontinuity in the system. Comparison was made with wave predictions based on an analytical model, and excellent agreement was found. The results suggest that, under the circumstances modelled, pressure wave-induced motion of syrinx fluid is unlikely to lengthen such cavities, unless the transverse tensile strength of cord tissue is even smaller than has been appreciated so far.

Keywords: Syringomyelia; Fluid–structure interaction; Wave transmission; Chiari malformation; Cerebrospinal fluid

1. Introduction

The pathological neurological condition known as syringomyelia has been recognised for over 130 years (Leyden, 1876). It comprises one or more fluid-filled cavities in the tissue of the spinal cord. By virtue of its interference with both motor and sensory nerves, the condition gives rise to highly variable symptoms which may include chronic pain, sensory deficit and paralysis. Such a cavity, or syrinx, is filled with fluid almost identical to the cerebrospinal fluid (CSF) that fills the subarachnoid space (SAS) surrounding the spinal cord. The neurology and neurosurgery professions distinguish between communicating and non-communicating syrinxes, and between canalicular and extra-canalicular syrinxes (Milhorat et al., 1997). The former distinction relates to whether the syrinx is open to the CSF-filled cranial ventricles and subarachnoid space via the small central canal of the spinal cord. In most adults, the central canal has become loculated, i.e. divided into multiple compartments lengthways by transverse membranes, so that canalicular location does not mean that the syrinx, an abnormally large-diameter part of the canal, necessarily communicates. Extra-canalicular syrinxes are usually located in the grey matter of the spinal cord, and do not communicate.

E-mail address: c.bertram@unsw.edu.au

0889-9746/$ - see front matter
doi:10.1016/j.jfluidstructs.2009.06.008

The majority of syrinxes are associated with a family of congenital abnormalities collectively known as Chiari malformation, in the commonest of which a herniation of the cerebellar tonsils of the hindbrain compresses the CSF pathways at the base of the skull. Syrinxes arising from this cause are generally found in the cervical spinal cord. Extra-canalicular syrinxes are commonly associated with past spinal trauma, and tend to be juxtaposed to the site of spinal scarring.

How such syrinxes initially form and subsequently enlarge is unclear at present, and accordingly surgical intervention to relieve the condition is often unsuccessful in the longer term. Hydrodynamic factors must play a large role, particularly given that the pressure in non-communicating syrinxes is often[1] found to be elevated at surgery. Since this paper concentrates on medium-to-large syrinxes, the following brief survey is restricted to possible mechanisms for enlargement; a comprehensive review is given by Klekamp (2002). Gardner (Gardner and McMurry, 1976) proposed that if the normal pathway from the fourth ventricle to the SAS was obstructed, cranial CSF pulsations (caused by arterial inflow to the head in systole) would be transmitted to a communicating syrinx via the central canal and dilate it. He believed that the narrow upper part of the central canal would act as a one-way valve, opening only during systole. In his 'suck' mechanism, Williams (1980) also hypothesized a one-way valve. He suggested that when a cough or sneeze caused pressure transmission up the SAS from the abdomen, the hindbrain tonsils allowed fluid into the head but not out. The raised cranial pressure would then force fluid down the central canal. Both theories thus attempt to explain raised syrinx pressure, but can only relate to communicating syrinxes, which are in the minority (Oldfield et al., 1994). Oldfield et al. (1994) suggested that the hindbrain tonsils, displaced downwards during systole if the normal systolic motion of CSF out of the head is obstructed, act on the SAS as a piston, increasing the amplitude of SAS pressure waves and thereby both supposedly forcing CSF into the cord tissue and massaging the contents of any existing syrinx caudally. The last part of this idea, the massaging, had already been termed the 'slosh' mechanism by Williams (1980, 1986, 1990), and it is the one with which this paper is particularly concerned. Williams, however, had in mind as the excitation source not so much the continual low-amplitude waves created by arterial systole in the head, which run caudally, as the occasional much-larger-amplitude waves starting abdominally caused by coughing (Williams, 1976), sneezing, straining or retching.

At the time when neurosurgeons devised these hypotheses, they could not be effectively tested. Since then, the topic has received attention from engineers, who have contributed new bench models of syringomyelia (Martin et al., 2005), application of mathematical theory (Berkouk et al., 2003; Carpenter et al., 2003; Cirovic et al., 2002; Wilcox et al., 2003) and analysis by numerical modelling (Bertram et al., 2005; Chang and Nakagawa, 2003; Loth et al., 2001; Stockman, 2006). The latter capability offers the opportunity to isolate and test the feasibility of suggested mechanisms under circumstances which, while they may be simplified relative to the anatomical reality, are at least exactly defined and quantitatively reasonable. Some of the clinical hypotheses are more readily suited to such examination than others. The various anatomic one-way valve hypotheses listed above are difficult to test, because their working or failure to work would depend on three-dimensional and highly patient-specific anatomic and material-property details. In contrast the idea that pressure waves passing along the SAS, and in the process moving intra-syrinx fluid along the syrinx (Park et al., 2008; Pinna et al., 2000; Sakas et al., 2005), might progressively lengthen the syrinx by cord tissue dissection, is one that can be tested in a rather general geometry, without the need for highly specific data on the geometry and mechanical properties of the patient's tissues. This is the approach taken here. The results, although not entirely conclusive, suggest that the forces induced by such motions would not dissect tissue under the circumstances dealt with here. In the process, useful and interesting details are revealed of the waves that are created by the interactions of the original excitation with the syrinx.

2. Methods

2.1. Anatomic model

As in previous modelling (Bertram et al., 2008, 2005), the finite-element fluid/structure-interaction code ADINA (ADINA R&D Inc., Watertown, MA, USA) was applied to create a fully interactive model of the CSF in the SAS, contained by the dura mater and its surroundings, with the SAS fluid in turn surrounding the spinal cord. The model

[1]For instance Stoodley has video evidence of fluid spurting from a syrinx at incision (2006, personal communication), and Milhorat et al. (1997) measured intra-syrinx pressures up to 22 cm H_2O. Hall et al. (1980) found that syrinx pressure exceeded SAS pressure in kaolin-induced syringomyelia. However, Williams (1976), who had made SAS pressure measurements in conscious humans, held that "The pressure in the syrinx cavity is commonly indistinguishable from the pressure in the subarachnoid space" (1986), and the intra-operative measurements of Heiss et al. (1999) support this.

includes a representation of the substantial syrinx shown by *in vivo* magnetic resonance imaging in Fig. 1. The fluid and structural parts of the model are shown in Fig. 2. The model is axisymmetric, so the syrinx is a slightly tapered cylinder, with conical ends of half-angle $\sim 23^\circ$, roughly as in Fig. 1. The main dimensions of the tapered cord and dura are unchanged from Bertram et al. (2008), and thus correspond to those indicated by the data of The Visible Human Project®. However, in an attempt to improve the caudal damping of waves, the model now includes for the first time a representation of the main dimensions of the *cauda equina* (horse's tail) where the sacral spinal cord becomes a bundle of anatomic nerves which exit the SAS separately. While this degree of detail is not included, the relatively sudden final tapering of the overall cord cross-section down to the collagenous *filum terminale* is reproduced, as is the slightly later inward tapering of the SAS (Crossman and Neary, 2005). Fig. 3 shows how the final cord taper also corresponds to the Visible Human data.

As before, the CSF (and now the syrinx fluid) was given the density, viscosity and bulk modulus of water. The mechanical properties of the tissues comprising the cord and dura were specified as for condition V2 by Bertram et al. (2008). The stiffness modulus was $E = E_0 + E_1 e^{-\beta_1 t}$, where $E_0 = 62.5$ kPa for the cord material and 1.25 MPa for the dura, $E_1 = 2E_0$ in both cases, and $\beta_1 = 2000\,\mathrm{s}^{-1}$. [Bertram et al. (2008) discuss how these values were arrived at from consideration of the published experimental data.] Functionally this amounts to a spring in parallel with a series spring/dashpot combination. The Poisson ratio was 0.49. For entry into ADINA, these viscoelastic properties were translated into equivalent values of viscoelastic shear and bulk moduli. These choices gave significant energy dissipation and a principal wavespeed of slightly over $7\,\mathrm{m\,s}^{-1}$, comparable with what has been measured using magnetic resonance imaging *in vivo* for the spinal cord (Kalata et al., 2009). The cord properties were maintained unchanged as the cross-section tapered inwards at the caudal end, but the ligamentous *filum terminale* was given the same properties as the dura.

Although coughing excites the spinal cord system abdominally, i.e. about two-thirds of the way down, for simplicity in the finite-element simulation, the FSI combination of models was excited by a short pressure transient applied at the open cranial end of the fluid model. As in previous work, a symmetrical triangular pulse of height 100 Pa (0.76 mmHg) and total duration 5 ms was used. This amplitude approximates what was measured by Heiss et al. (1999) in response to cranial arterial pulsation, but the resulting rise-rate of 304 mmHg/s is reminiscent of coughing. Lumbar SAS pressure rise-rates of 212 ± 73 mmHg/s were measured for cough in normal volunteers by Sansur et al. (2003); Chiari I patients were not significantly different. Coughing produces much larger amplitudes (Williams, 1972), but since the model was

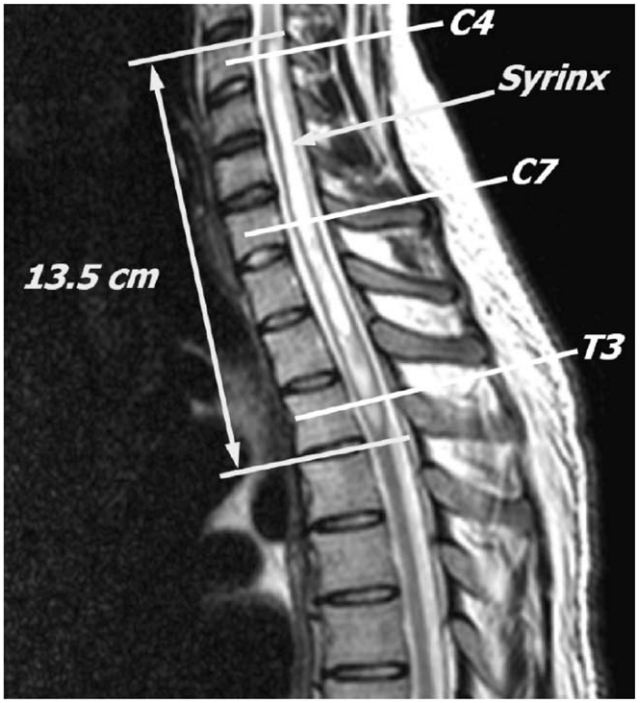

Fig. 1. MR image of a large syrinx in the cervical spinal cord of a human, with dimensional indicators overlaid. Reproduced from Martin et al. (2005) with permission of the American Society of Mechanical Engineers.

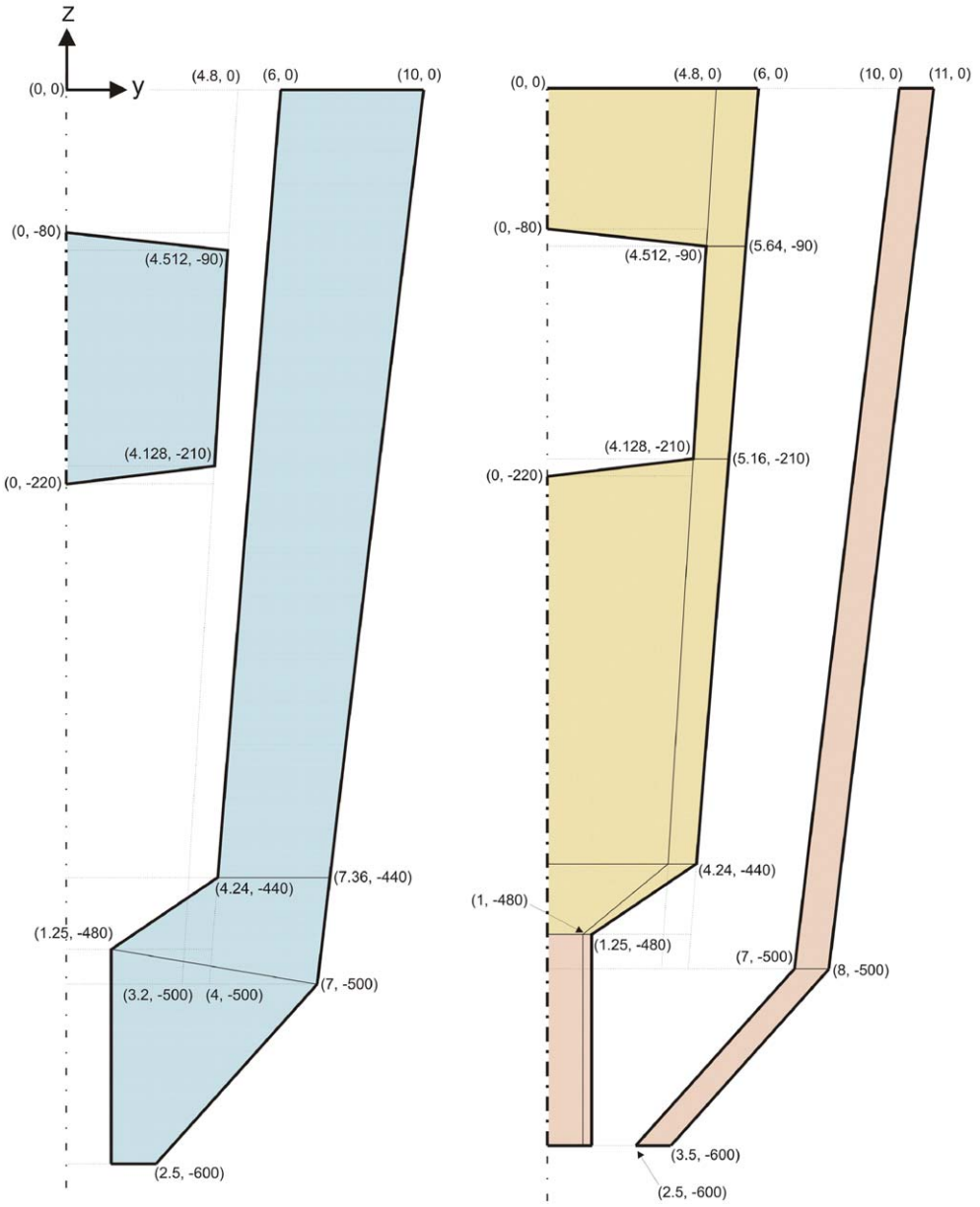

Fig. 2. Outlines of the two-dimensional axisymmetric fluid and structure models set up for finite-element simulation. The parentheses give y, z-coordinates in millimetres, where y is radial and z is axial. The figure shows radial dimensions scaled up 20 × relative to axial distance; thus the true taper of the conical ends of the syrinx was a half-angle of about 23°.

linear, responses can be proportionally increased. The pulse was deliberately brief to reveal wave propagation details. The excitation produced by a cough lasts longer (Sansur et al., 2003).

The narrow caudal end of the fluid model was closed off by a rigid fixed wall. The structure model was likewise clamped in position at the caudal end, and also at the cranial end.

2.2. Extended models

To allow examination of the various waves in separate detail, FSI models were also constructed with all longitudinal dimensions (except the tapered ends of the syrinx) increased by a factor of three. These models were untapered, having

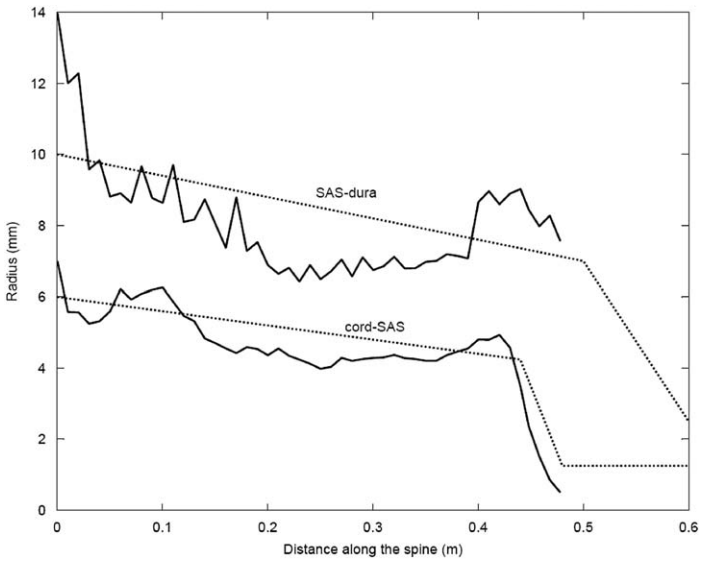

Fig. 3. Comparison of the dimensions of the SAS, as modelled complete with sacral cord-ending structures, with computed tomography data from the Visible Human project, processed to reduce the three-dimensional transverse body cross-sections to equivalent radii.

the radial dimensions of the anatomic model halfway along the uniformly tapered section, and did not include any reproduction of the cord-ending structures. Three basic models were used: (i) with a syrinx of proportionally increased length, (ii) without a syrinx, and (iii) with a continuous syrinx all the way along, so that the 'cord' became a simple cylinder of the same wall thickness as the lengthened cylindrical 'dura'. Thus the cord in this model had inner and outer radii of 4 and 5 mm, the dura, 8.5 and 9.5 mm.

2.3. Numerical details

The anatomical model contained 6528 4-node fluid cells and 1248 9-node solid cells; extended model 1 contained 16 704 and 3024 cells respectively. These numbers allowed the vertices of the rectangular fluid and solid cells to match along the FSI boundaries, with one solid cell abutting two fluid cells along each shared side; although ADINA does not strictly require this, it provides maximum likelihood of avoiding fluid/structure grid overlap. Solid cells were uniformly distributed; fluid cells were biased towards the inner and outer walls of the SAS so as to improve resolution of the shear layers. The geometrical treatment generally followed that used by Bertram et al. (2005); grid-density variation tests therein showed that results were to a very good approximation grid-independent.

Each simulation involved solving 200 FSI time-steps of 0.5 ms. The time-integration method used here was ADINA's second-order-accurate composite scheme, which involves a predictor–corrector approach of two sub-steps. Again, tests with variation of the time-step length have shown previously that the results are time-step-independent.

2.4. Analytical comparison

The excitation gave rise to multiple waves of differing speed. Wavespeed was estimated by plotting quantities such as $p(z,\ t)|_{y=k}$, where p is pressure, t is time, y and z are radial and axial coordinates, and k is a constant, as shaded contours and fitting the best straight line by eye. The slope of the line then gave speed. Since the induced waves were short and isolated, giving rise to a narrow track on such plots, this procedure was not subject to systematic error from wave attenuation, as it would be if applied to the leading edge of waves of longer duration. These numerical wavespeeds were compared with analytical predictions based on equations adduced by Cirovic (2009). The equations predict the speed of four waves expected in a system of two coaxial flexible annuli with a fluid between them and filling the cylindrical space inside the inner one. This is a model of the dura, SAS, cord and central canal. Based on previous work (Bertram et al., 2005) indicating that the effect of the central canal on propagation is insignificant, the equations were here solved (using Matlab) for a vanishingly small central-canal radius, and also for a central radius corresponding to that of the syrinx when this was included. All other quantities conformed to those used in the finite-element simulations.

The equations assume a single fixed value for the elastic stiffness of each material; the value used was that corresponding to E_1 in each case.

3. Results

3.1. Anatomical model

Fig. 4(a) shows the result of exciting the fluid model with a short pressure pulse applied at the cranial end ($z = 0$) of the SAS, in terms of the radial stress $\sigma_{yy}(z, t)$ on the cord axis ($y = 0$) in the solid model. The region occupied axially by the syrinx ($-0.08 > z > -0.22$ m) is therefore empty. Three primary waves are apparent. The strongest (dark blue on-line, indicating radial cord compressive stress) is also the slowest, reaching the filum after some 60 ms. As expected on the basis of equations provided by Bertram et al. (2005), its speed varies along the model, increasing as the model tapers inwards. A second, weaker (at least in terms of the plotted quantity) wave (light blue on-line) propagates somewhat faster, arriving at the filum in around 35 ms. The third wave (in terms of cord-axis radial stress magnitude) is fastest, reaching the filum in about 11 ms. All three waves pass the region occupied by the syrinx without major apparent change, but reflections are generated by waves incident on the cranial end of the syrinx region, which then return to the cranial end of the model and are there re-reflected. When the first wave arrives at the caudal end of the syrinx region, it splits, giving rise to a new wave which travels at the higher speed of the second wave and therefore arrives earlier

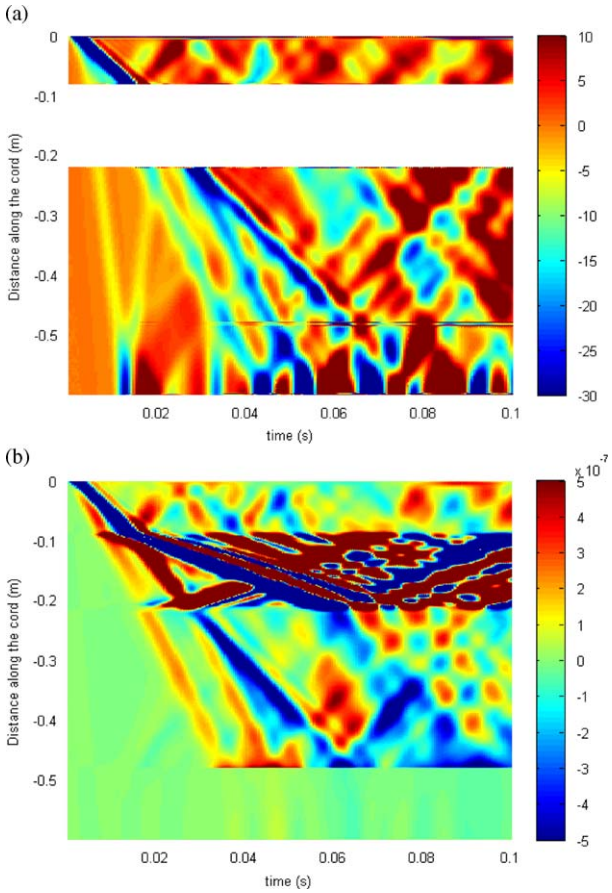

Fig. 4. Waves in the cord during the first 100 ms after the start of an excitation pulse. Distance along the cord is measured from the cranial end of the model. (a) Radial stress (Pa) on the cord axis. Since these data come from the solid model, the region occupied by the syrinx is blank. A line of stress concentration is seen at $z = -0.48$ m, where the end of the cord becomes the filum. (b) Radial displacement (m) beneath the cord surface, at the (slowly varying) radius of the syrinx boundary.

(~47 ms) at the filum. Further wave reflections occur at the cord/filum interface and at the caudal end of the model, so that the overall picture becomes confused. It is however clear that the cord-ending structures, including the inward-tapering final part of the SAS and the filum, are ineffective as a means of absorbing waves and preventing their reflection back into the main part of the model.

Although $\sigma_{yy}(z, t)$ showed some of the complexity of the wave travel created in the system by the initial excitation, by reflection and by wave-splitting, it does not show all. A rather different picture is revealed (Fig. 4(b)) by plotting the radial displacement $\Delta y(z, t)$ of the intra-cord line corresponding to the outside radius of the syrinx, extended all the way up and down the cord. Because of the cord taper, this position does not correspond to a single value of y. While the first and second waves (and the splitting of the first wave) noted from $\sigma_{yy}(z, t)$ are still visible distal to the syrinx, the picture is dominated by very slow waves passing along the syrinx border, i.e. the thin annulus of remaining cord over the syrinx. Such waves are created when the first and second waves arrive at the proximal end of the syrinx, but also when these waves pass the distal end they cause new slow waves to propagate back along the syrinx margin. Yet more forward-going slow waves are generated when the waves reflected back to the origin off the start of the syrinx region arrive at the syrinx a second time. When forward-going slow waves reach the end of the syrinx, they appear to reflect essentially all of their energy back into the syrinx region, as further slow backward-going waves. Because of the thin and therefore highly flexible sheath of cord over the syrinx, all of these slow waves in the syrinx region cause much greater Δy than any waves in the pre- or post-syrinx regions. Conversely, the radial displacements of the rather stiff filum are negligible; there is an abrupt change in displacement amplitudes at the cord/filum interface and at each end of the syrinx.

From the radial-displacement findings combined with the radial-stress results illustrated, it becomes clear that both the first and second waves are greatly slowed as they pass the syrinx, from 7.6 and 14.75 m/s elsewhere to 2.9 and 9.2 m/s past the syrinx. As will be discussed further below, the first wave has the character of a Young wave (consisting primarily of extra fluid pressure creating radial cord compression and dural distension).

As might be expected, the very slow waves are much less in evidence when $\Delta y(z, t)$ is plotted for the inside edge of the dura as in Fig. 5(a). Prominently, much of the energy of the second wave continues past the syrinx without change. The first (Young) wave splits when it reaches the proximal end of the syrinx into a very slow Young wave and a dominant type-2 wave; thus the effect is an apparent speed-up from 7.6 to 9.2 m/s. When this wave reaches the distal end of the syrinx it splits again, into components of roughly equal strength at the two non-syrinx wavespeeds.

The third and fastest wave is not significant in terms of dural radial displacement. However, when fluid pressure at the outside edge of the SAS is plotted as $p(z, t)$ as in Fig. 5(b), it shows up clearly, passing the syrinx apparently without interaction at an unchanged wavespeed of 57 m/s.

3.2. Results pertaining to slosh

Fig. 6 shows pressure $p(z)$ from the fluid model at three salient times during the 100 ms investigated. Each panel shows a comparison between the pressure of the CSF in the SAS and the pressure of the syrinx fluid. At 8 ms, the syrinx pressure mimics that in the SAS over most of its length, but at the upstream end, the syrinx pressure is twice that in the SAS. This time is shown because it is when syrinx pressure at the upstream end first peaked. Thanks to wave dispersion (the creation of three waves), the 100 Pa excitation has already decayed insofar as the main wave is concerned to a peak of less than 80 Pa. At 23 ms, the pressure three-quarters of the way along the syrinx is higher than anywhere in the SAS; this time is shown to illustrate what was a rather consistent relationship between SAS and syrinx pressures as the main wave passed the syrinx; the peak intra-syrinx pressure was maintained some 25% higher than that in the adjacent SAS. At the caudal end, the syrinx pressure is again higher than that in the adjacent part of the SAS, a situation that lasted from 19.5 ms until at 29 ms the main wave had passed the whole syrinx. Note that the simulation computes pressure relative to the constant pressure existing everywhere in the model in the absence of excitation; thus, negative values simply mean that the pressure is locally and temporarily lower than that starting value. At 67 ms, the SAS pressure is high at the caudal end of the model; this is when the main wave is arriving and starting to be reflected from the end of the SAS. However, the feature of most interest is the extent to which the pressure at the caudal end of the syrinx exceeds that in the adjacent SAS, reaching some 48 Pa at this time.

Fig. 7(a) shows the pressure generated at each end of the syrinx by the passage of the various waves and their reflections following the impulse at the cranial end of the SAS. No excitation is applied directly to the syrinx, yet the pressure therein reaches a maximum at the caudal end only just short of the 100 Pa initial SAS excitation. Fig. 7(b) shows the corresponding radial stresses generated in the cord tissue at each end of the syrinx (on-axis). Because the geometry includes a sharp conical tip to the syrinx cavity, the stress in the solid cannot be fully resolved at this point, and so the figure includes also curves showing the radial stress one grid point back from the tip of the syrinx. Owing to the varying pressure in the SAS, the radial stresses in the cord at the syrinx tips do not closely follow the pattern of the

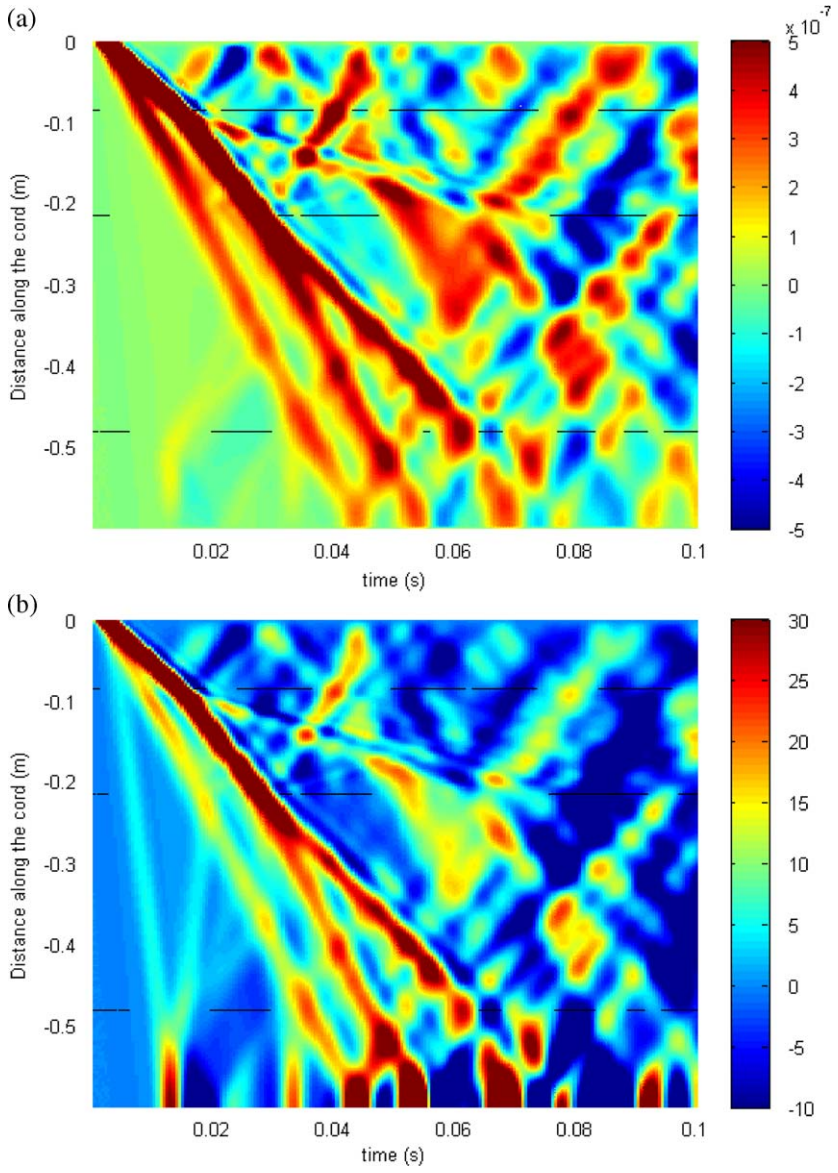

Fig. 5. Waves at the inner edge of the dura. Interrupted horizontal lines indicate the approximate axial position of the beginning and end of the syrinx and the start of the filum. (a) Radial displacement (m), from the solid model. (b) Pressure (Pa), from the fluid model.

pressure in the intra-syrinx fluid adjacently. The crucial issue is the extent of positive, i.e. tensile, radial stress in the cord material; this is potentially the stress which can tear the cord material, thus extending the syrinx according to the 'slosh' hypothesis. At no time does the tensile stress reach the magnitude of the initial SAS excitation. The peak tensile stress cranial to the syrinx is ~65 Pa at the nearest grid point or ~32 Pa at the next one back, whereas the peak fluid pressure at the cranial corner of the syrinx was ~54 Pa (at this same instant). At the caudal end, because of concomitant pressure in the SAS, the syrinx fluid pressure peaks are not accompanied by exceptional cord radial stress. The maximum positive radial stress reached there at any time is relatively small, and occurs late on when waves reflected from the end of the cord, the extent of which may be artefactual, dominate.

Slosh as defined by Williams is the axial transfer of fluid, basically from one half of a syrinx to the other. This process can be quantified in the model by examining the axial velocity of fluid across a transverse line that cuts the syrinx into two equal-length pieces (in 3-D this line would correspond to a surface). Because the solid but flexible parts of the model are also set in motion by the excitation, it is necessary to distinguish between motion of the syrinx itself and motion of

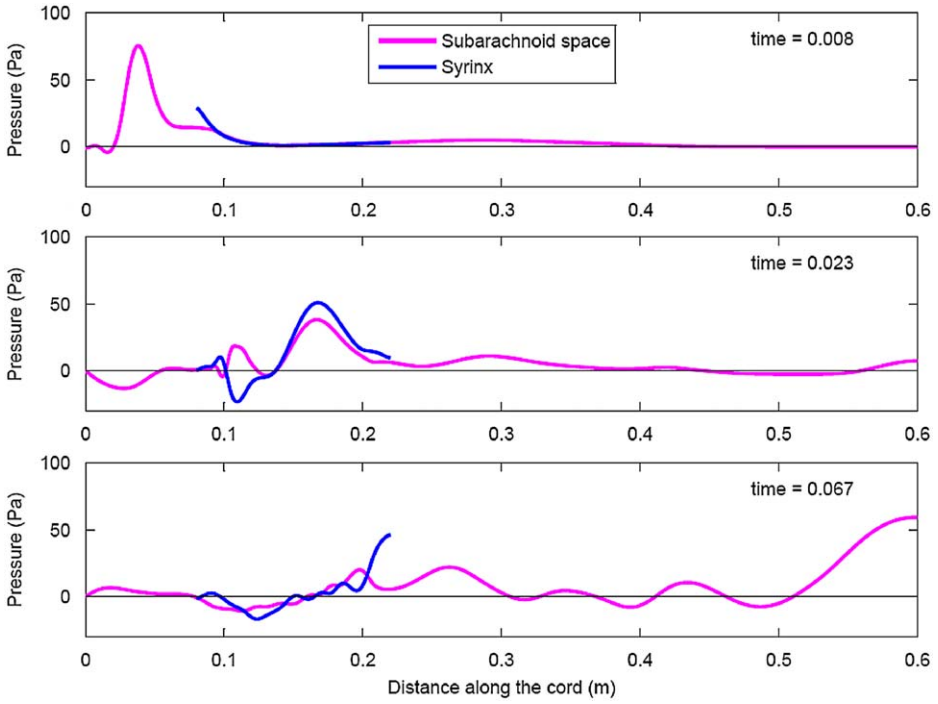

Fig. 6. Comparison of pressure in the SAS with pressure in the syrinx, at three different times following excitation with a short 100 Pa pulse at $t = 0$, $z = 0$.

the fluid within. Fig. 8(a) shows the axial velocity of syrinx fluid crossing the cut on the axis of model axisymmetry ($y = 0$), and also shows the simultaneous axial velocity of the wall of the syrinx at this same axial location ($z = -0.15$ m initially). Fluid velocity relative to a stationary frame is what would be detected by phase-contrast magnetic resonance measurement. The peak axial-velocity magnitudes for the syrinx and contents are comparable; the centre-line fluid velocity[2] reaches 7 mm/s at 37 ms, while the local syrinx wall velocity reaches 5 mm/s at 21 ms. However, the actual slosh velocity is the fluid motion relative to the wall. This, the difference between the two curves in Fig. 8(a), is shown in Fig. 8(b). With the fluid and syrinx motions out of phase, the peak slosh velocity of 10.4 mm/s occurs when the syrinx and fluid within are moving in opposite directions, at 21 ms. The syrinx end-pressures engendered by the slosh depend mainly on this relative motion; the peak pressure at the caudal end, at 27.5 ms (Fig. 7(a)), is a slightly delayed consequence of the peak (caudally directed) slosh passing the syrinx midpoint.

3.3. Extended models

The incident waves in Fig. 4 are so rapidly overlaid by reflections as to be difficult to track, and measurement of their wavespeed was correspondingly imprecise. The creation of a model with total and syrinx length increased three times overcame this problem. Fig. 9(a) shows the radial displacements $\Delta y(z, t)$ seen all along the lengthened cord at the radius of the syrinx. Apart from the fastest wave, which is not visible in this presentation, waves do not now reach the end of the cord before the end of the 100 ms window. Even without reflections from the caudal end, there are at least 25 distinct waves visible in this picture, of which a detailed analysis will be given below. However, a few general conclusions can be drawn at this stage. Only some of the waves are affected by the syrinx. For those that are, the process of onward transmission induces splitting of the energy into onward waves of unequal speed. Similarly, reflection (from either one of the syrinx ends or from the cranial model end) in general gives rise to more than one returning wave through a similar splitting process. The very slow forward-travelling waves generated in the thin cylinder of cord material overlying the syrinx are of particularly large amplitude. However, if radial displacement is instead plotted for the inside edge of the dura (not shown), these waves are almost absent.

[2]The centre-line value did not greatly exceed the mean; the velocity profile was in all cases distinctly flat other than close to the wall.

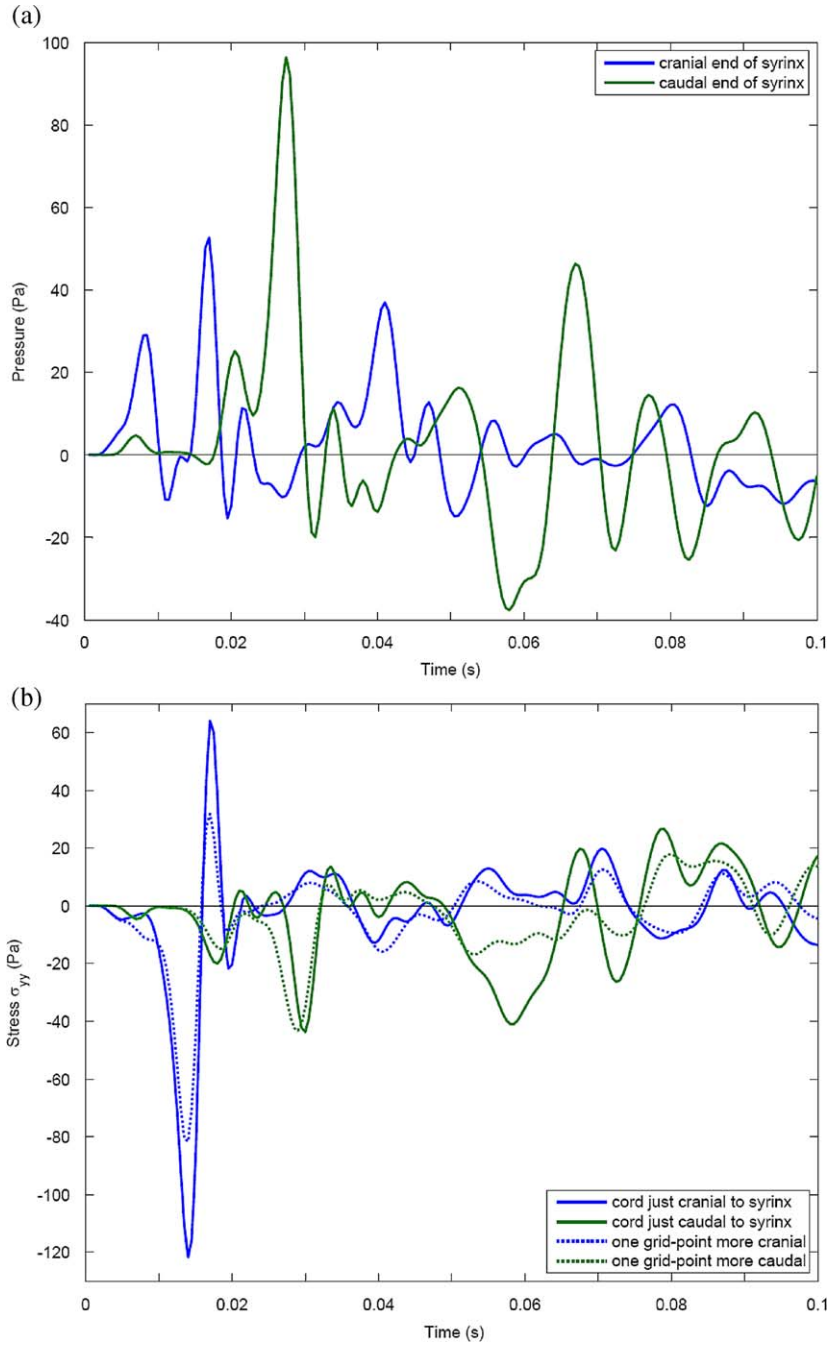

Fig. 7. (a) Fluid pressure at each end of the syrinx. (b) Radial stress on-axis in the cord just cranial and just caudal to the syrinx.

Plotting radial stress at the cord axis (not shown), the fastest wave was seen to make two round trips from the cranial to the caudal end and back inside 0.1 s, apparently without any interaction with the syrinx. This wave is still more advantageously seen by plotting $p(z, t)$ at the inside edge of the dura as in Fig. 9(b). It can then be seen that the arrival of the slowest wave back at the cranial end of the cord after reflection from the leading edge of the syrinx leads to the creation of a faint new forward-going fastest wave. Since 'pressure' in the solid is computed as minus the average of the radial and axial normal stresses, it is natural to enquire which of these two stresses contributes more to the fast-wave pressure. The comparison showed that subdural axial stress is a potent carrier of this wave. Thus the fast wave is a

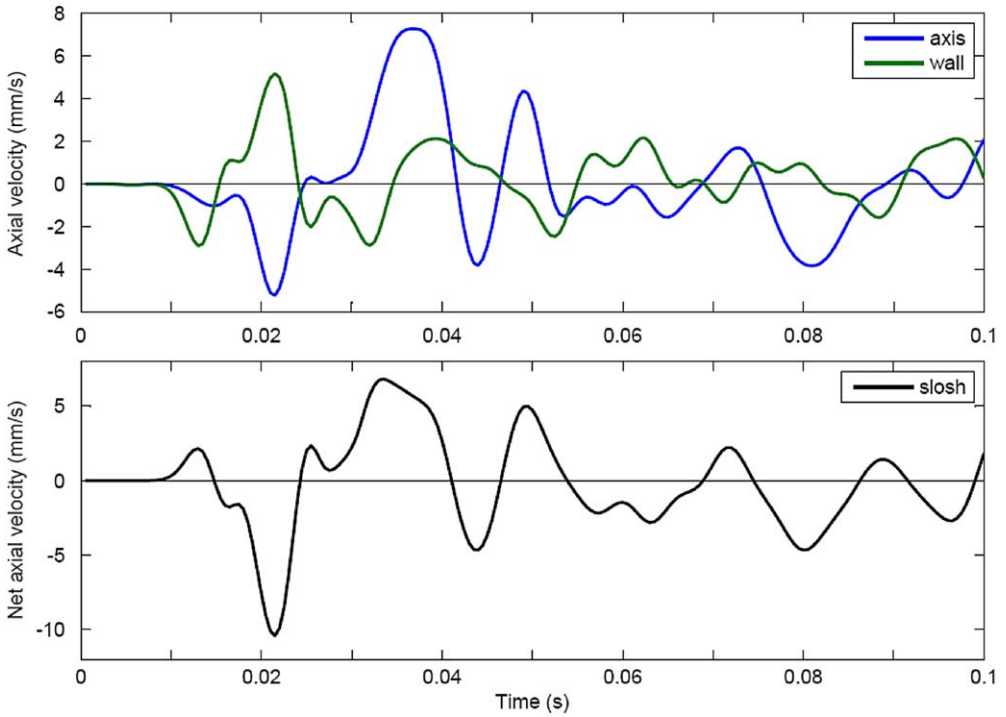

Fig. 8. Axial fluid velocity at the middle of the syrinx. The upper panel shows the centre-line velocity as it would be recorded by magnetic resonance imaging, i.e. in laboratory coordinates, and also shows the simultaneous axial velocity of the syrinx wall at this level. The lower panel shows the difference between these two curves; this is the centre-line of the flow from one half of the syrinx to the other, i.e. the 'slosh'. Positive values of velocity are cranially directed.

Lamb wave travelling in the dura, consisting of a transient of axial tensile stress arising from the initial excitatory stretch.

The wavespeeds measured in this model are in excellent agreement with those predicted by solving the equations provided by Cirovic (2009), as shown in Table 1. With the aid of the systematisation provided by the comparison in Table 1, essentially all the waves visible in Fig. 9 can now be ascribed to their origin in one or other of the incident waves provoked by the original excitation, as shown in Fig. 10. All the waves here are colour-coded according to which incident wave was responsible for their creation. Thus ultimately, through the wave-splitting that occurs when waves are reflected at the cranial end of the model, fast (c_4) waves are present which relate to incident waves 2, 3 and 4. The predicted incident wave 1 was not found in the lengthened numerical model of cord and syrinx. It became manifest only once the waves had been refracted to slower speeds while passing the syrinx. As shown in Fig. 10, its predicted speed in the solid cord part of the model was not substantially different from wave 2, so its detection in even the greater distance afforded in lengthened model 2 was impossible, appear to given the finite distance occupied by each wave transient.

Incident wave 2 was refracted by the syrinx ends and reflected both by the syrinx ends and by the cranial end of the model. Through these processes, new waves of types 1–4 were created. The same can be said of incident wave 3, but additionally a component of this wave was unaffected by the syrinx. Incident wave 4 did not interact with the syrinx, and its reflection at the ends of the model did not appear to give rise to slower waves.

Fig. 9 also shows details of the polarity of some of the refraction and reflection events, i.e. whether waves are refracted/reflected in-phase or inverted. While the majority of refracted and reflected waves retained the polarity of their incident progenitor, incident wave 2, which was a transient of radial cord compression, i.e. reduction in cord radius, gave rise to a prominent onward-transmitted wave of type 3, which consisted of cord radius increase. This in turn spawned an onward type-2 compression wave when it exited the syrinx region. However, if looked at in terms of radial displacement of the inside edge of the dura (not shown), this trio of wave components all created transient dural radius increase. Thus the type-3 wave passing the syrinx was not a simple inversion of the type-2 wave elsewhere. Many other instances of waves changing character occurred; consequently (for example) the pattern of waves ricocheting in the

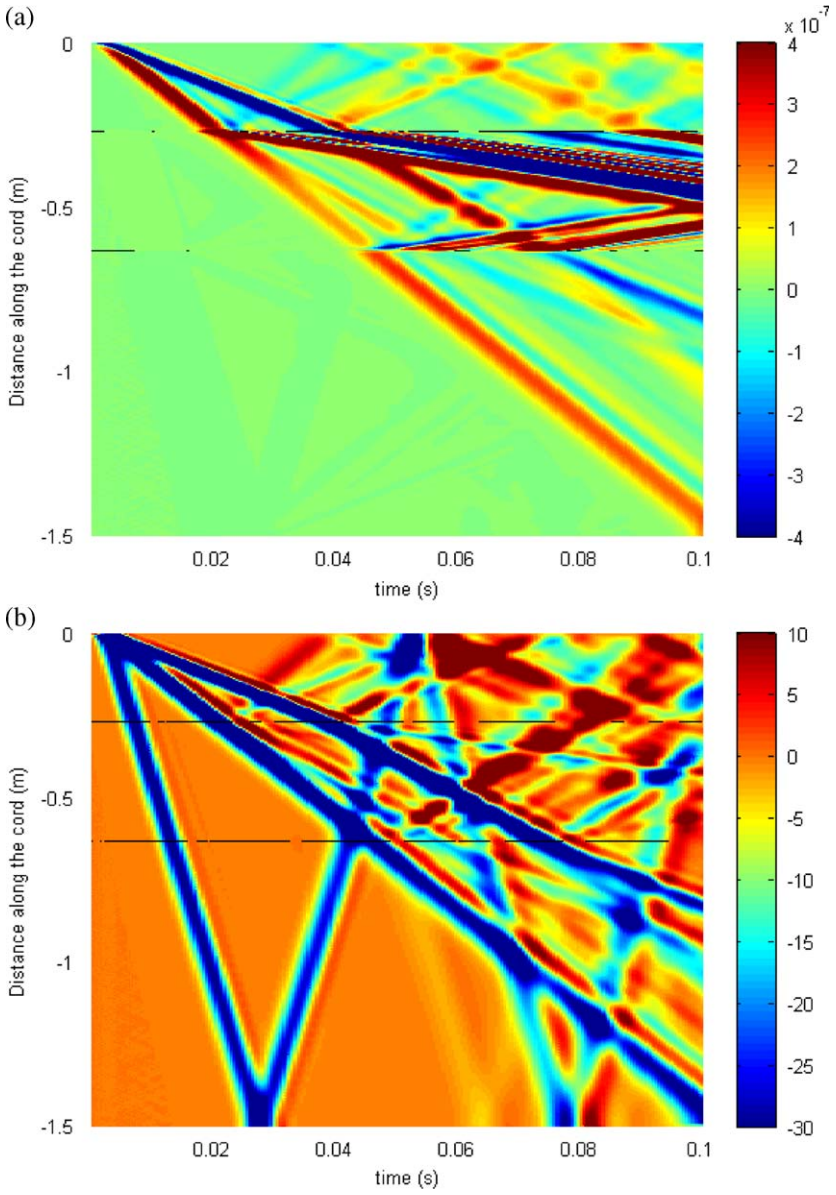

Fig. 9. (a) Radial displacements (m) in the untapered lengthened model of cord and syrinx, at the radial level of the syrinx radius, i.e. below the cord surface and within the cord material except where the syrinx occurred. Interrupted horizontal lines indicate the axial position of the lengthened syrinx. (b) Pressure (Pa) in the solid model at the inside radius of the dura.

model section cranial to the syrinx start as seen in terms of dural radius change was not the inverse of that in the same section viewed in terms of cord radius change.

Using a specific set of parameter values thought representative of spinal cord dimensions and properties (but leading to higher wavespeeds than those modelled here), Cirovic (2009) was able to conclude by comparison of induced tube and fluid axial velocities associated with each wave type that type-1 and type-4 waves were the most and least significant, respectively, in terms of CSF movement. The type-1 wave was found to be essentially a Young wave in the cord, type-2 and type-3 waves involved varying degrees of coupling of the cord and dura, and as already concluded here, the type-4 wave was a Lamb wave in the dura. By means of the numerical simulations here, it is now possible to see explicitly the nature of each of the waves in terms of the resulting deformations of the model. To allow the type-1 wave to become apparent, for this purpose an untapered lengthened model consisting of all syrinx was constructed.

Table 1
A comparison of wavespeeds measured from the lengthened model of the cord and syrinx with those predicted by solving the equations of Cirovic (2009).

Wave	Solid cord		Cord + syrinx	
	cord10d	Cirovic	cord10d	Cirovic
c_1		6.5	3.0	2.9
c_2	7.3	7.3	10.9	10.2
c_3	14.5	14.2	(14.5)	13.6
c_4	57	56.8	(57)	56.8

The numerical wavespeeds were measured by manual best-fitting of a line to the track of the corresponding wave on plots of $p(z, t)$, etc. Numbers in parentheses indicate that the corresponding wave was not obviously altered in speed past the syrinx, and its speed was taken as being the same as in the solid cord.

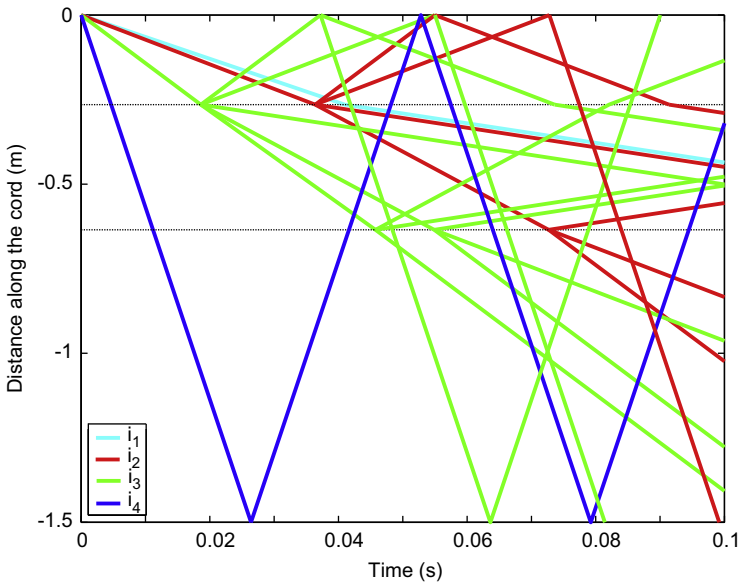

Fig. 10. All the waves found in the lengthened model are here explained in terms of refraction and reflection at the ends of the syrinx (shown by horizontal lines) and reflection from the cranial and caudal ends of the cord. Waves are given one of four colours as in the legend, based on the original incident wave which is responsible.

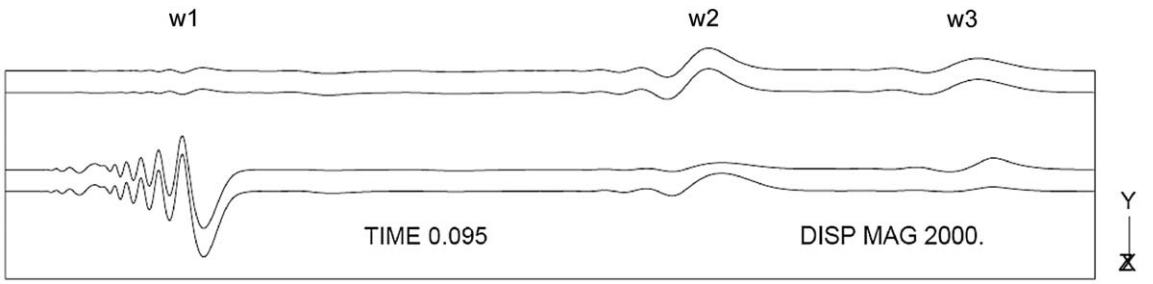

Fig. 11. Waves of types 1, 2 and 3 are here shown travelling from left to right in a lengthened model which includes a syrinx extending along the whole model. The radial length scale (here, vertically upwards from the axis of axisymmetry at the bottom of the figure) is exaggerated 30 times relative to the axial scale in this representation. Wave-created displacements are here magnified by a factor of 2000. The model was excited by a single transient applied at the 'cranial' (left-hand) end.

Fig. 11 shows incident waves 1, 2 and 3 travelling from left to right in this model. Type-4 waves did not create radial displacements of comparable magnitude, and are accordingly not clearly visible on this scale, although their subtle presence could be noticed in an animation of similar deflection plots as time progressed.

Bertram et al. (2008) described the waves in a model without a syrinx as Young and Lamb waves, corresponding to primarily radial and axial particle displacements, respectively. Already that was something of an extrapolation, since the only model for which that nomenclature would be exact is one without a cord. Once a syrinx is added, the system consists of two concentric elastic annuli enclosing fluid, and is sufficiently specialised that no recognized scientific names for all the resulting waves exist. The extremely slow wave 1 still clearly has predominantly the character of a Young wave, creating principally a transient of increased pressure in the SAS, inward deflection of the greatly thinned cord overlying the syrinx, and much smaller outward deflection of the stiff cylindrical dura. This wave was also associated with a transient reduction of syrinx pressure, and generated a prominent series of after-runners. Wave 2 is the most significant in terms of dural deflection; it also created the most pressure in both the syrinx and the SAS. Emphasising its completely different character from wave 1, the outward dural deflection is accompanied by outward cord deflection. Wave 3 is superficially similar to wave 2 in this respect, but differs in that the outward cord deflection is associated with local cord thickening, as a result of high axial compressive stress and much smaller radial compressive stress, whereas wave 2 led to local cord thinning by simultaneous radial compression and axial extension. Wave 4 is essentially a Lamb wave in the dura; it consisted principally of dural axial tensile stress (all the others created compressive dural axial stress). All four waves caused compressive radial stress in the dura, with wave 4 as significant as wave 1 in this respect.

4. Discussion

As indicated in the Introduction, numerical simulations are necessarily a simplification of what is found *in vivo*. In this case, the assumptions include axisymmetry and isotropic linearly elastic solids. The so-called anatomical model was excited by a small short isolated pulse of pressure at the cranial end, i.e. at the level of the hindbrain, where the model terminated and was immobilised. The model omitted anatomical details such as nerves branching from the cord and the denticulate ligaments, as well as wall irregularities. However, the advantage of numerical modelling of the spinal cord system, with fluid/structure interactions accounted for, is that the resulting predictions are well-founded physically under the circumstances documented. In this they differ profoundly from mere qualitative speculations, which, through ignoring quantitative factors, being selective about the mechanics considered, and inability to predict the interactions of multiple phenomena, may lead to wholly erroneous outcomes. A numerical model of the subarachnoid space and its flexible bounding solids may not cover the pathology that interests a particular reader, but what it does and does not include is clear, and (provided that the numerics have been competently handled) the results are the indisputable consequence of those inputs. In comparison, experiments *in vivo* include myriad covert factors which may govern the findings, and even experiments *in vitro* are prone to influences which may go unreported because their importance was not recognized by the experimenter.

The results of this particular investigation suggest that 'slosh' may not generate sufficient force to lengthen a syrinx. Waves travelling in the SAS certainly produce detectable slosh, but its slight magnitude matters, a point that sometimes seems to be overlooked in the clinical literature. There was (as has been measured *in vivo*) only relatively low-speed flow to the caudal end of the syrinx. Axial syrinx fluid motion has been quantified by phase-contrast cine magnetic resonance imaging (Brugières et al., 2000; Heiss et al., 1999; Martin et al., 2005). A caudally directed systolic peak of just under 20 mm/s was measured by Brugières et al. in large cord systs as a result of arterial pulsation; Heiss et al. measured a peak of 17 mm/s. Thus the peak slosh velocity of 10.4 mm/s predicted here, for an excitatory pressure which may have been slightly smaller than that present in the patients examined by Brugières et al., is well within a factor of two of that measured *in vivo*. The pcMR results suggest that axial cord motion is small relative to both SAS and syrinx fluid motions, so it is appropriate to compare the peak slosh (relative) velocity rather than the peak absolute velocity, because the relative motion here would approximate the absolute motion if the syrinx were more stationary. The fact that comparable magnitudes of fluid and syrinx motion were predicted here is probably due to the lack of cord-to-dura tethering by denticulate ligaments and dura-to-spine tethering by fat in the model.

The reason why SAS pressure-wave propagation produces relatively little slosh is now clear: despite the greatly reduced speed of the slowest wave past the syrinx, the wavespeeds remain too distant (essentially three orders of magnitude) from the speed of axial motion that the initially and basically stationary syrinx fluid achieves. The mechanism amounts to a peristaltic action of the waves being supported by the syrinx/cord/SAS/dura system on the bulk advection of the syrinx contents. However, the mechanism is rather ineffective, both because the peristalsis amplitude remains small when (as here) reasonably realistic quantitative parameter values are used for the geometry and material properties, and because of the large wavespeed/fluid-speed disparity.

The slosh elevates the fluid pressure at the downstream end of the syrinx when the inertia of the moving fluid is resisted by the tissue at the end of the syrinx; essentially the momentum of the fluid becomes force on the cord. However the slosh, which has been shown to be comparable to that observed *in vivo*, was insufficient to create high pressures or stresses. The fluid pressure at the downstream end of the syrinx remained modest, and the radial tensile stress (i.e. tearing stress) in the cord material at this point did not significantly exceed the value of the fluid pressure. In view of the somewhat tapered ends of the syrinx in Fig. 1, the model syrinx was deliberately given conical ends of roughly the same aspect ratio, to allow for the possibility of exaggerated stresses. In principle, such a geometry allows a stress concentration at this point, as occurs at the apex of a crack, but significant stress concentration was not predicted. In any case, whereas a crack is linear and free to propagate, propagation of an axisymmetric conical cavity tip in any direction is well resisted by the surrounding material.[3] While the model did not fully resolve the stresses right at the apex of the syrinx ends, Fig. 1 also suggests rounded ends, which would reduce stress concentration. Both for this reason and because linear cracks could not be simulated, further grid refinement at this location was not merited.

All values of deflections, pressures and stresses simulated here could be multiplied by a factor of 100 to represent the maximum amplitude of SAS wave excitation in coughing (Williams, 1976). However, the maximum radial tensile stress thus predicted at the ends of the syrinx (in the approximate range 3–6 kPa) would still not approach the tearing stress of the cord material, which to a first approximation can be taken as equal to the elastic stiffness modulus used here (62.5 kPa). Nevertheless, the latter value, while appropriate to the overall properties of the cord as indicated by measured wavespeed and other data, may overlook important detail. The cord was here treated as a single isotropic linear viscoelastic material. In reality the cord consists of an extremely pliant, barely solid material within a very thin but tough membrane, the *pia mater*. Mazuchowski and Thibault (2003) and Ozawa et al. (2004) have shown that the properties of the cord with and without the pia differ greatly. A second reason to be cautious is that our knowledge of cord properties is almost entirely drawn from axial tensile and transverse compressive testing. It may be that the interior cord material has negligible ability to withstand transverse or radial tensile stress; Ozawa et al. (2001) measured rabbit cord material stiffness modulus values of the order of 3 kPa by pipette aspiration, although they acknowledged that their cut sections might not typify *in vivo* values. Thus it is possible that even the low pressures and tensile radial stresses implied by the simulations here may suffice in some cases to lengthen an existing syrinx. However, slosh velocities of the order implied by this degree of scale-up have not been observed.

The conclusions reached regarding slosh are not weakened by the use of an isolated short pulse, administered cranially, which does not correspond closely to either a cough or an arterial pulse. The results do not depend on the slight degree of taper, which was the only factor that differentiated caudally directed wave travel from cranial. To maximise the separation of individual waves, the pulse used here was short, and created frequencies as high as any to be expected from even the most percussive of coughing. The constant gentle excitation provided by arterial pulsation in the head does not include such high frequencies. Both arterial pulsation and coughing produce pressure pulses that last much longer than the pulse used here. However, slowly varying excitations only cause all parts of the system to change pressure in unison (Bertram et al., 2005), and will not produce additional syrinx peristalsis, at least in the absence of SAS stenosis. It is the highest frequency components of the excitation, which, by creating waves of shorter wavelength than the syrinx itself despite the high wavespeed, urge syrinx fluid motion. Thus the predicted slosh velocities here were of the same order as those measured *in vivo*, despite the brevity and relatively small amplitude of the excitation.

This is not to say that longer-lived excitations may not have an indirect influence on the extent of slosh. Williams himself suggested two ways in which this might occur. Coughing excites waves in the subarachnoid space by compressing it abdominally via distension of the epidural veins. He suggested that this might in turn cause the simultaneous local compression of part of a suitably located long syrinx. As noted already, coughing creates a transient of rapid onset, but one with a relatively slow decay (Sansur et al., 2003; Williams, 1976). If this leads to relatively prolonged compression of the aforesaid syrinx part, substantial fluid displacement toward the rest of the syrinx could potentially occur. However, it is important to note how even this relatively simple hypothesis includes components which have not been tested.

Williams' second suggestion brings in his other hypothesis, 'suck'. He documented, through pressure measurements in conscious patients, a number of situations in which manoeuvres such as Valsalva produced in their aftermath substantial 'pressure dissociation', i.e. pressure difference between the cranial and spinal subarachnoid space. The pressure difference was slow to decay when axial subarachnoid flow was impeded by, for instance, a hindbrain tonsil regaining its SAS-blocking position after (it was assumed) being temporarily displaced upwards during the manoeuvre. Again this suggested that a suitably located syrinx, in this case one spanning the bottom margin of the skull in a Chiari I

[3]This is not simply an issue of axisymmetric modelling over-simplification. Given the extent to which a syrinx such as that shown in Fig. 1 approximates axisymmetry, as does the cord containing it, there is a real question as to whether conventional crack propagation theory is relevant. To the author's knowledge, the axisymmetric situation has not been analysed theoretically.

malformation, would be subjected to a relatively prolonged compression of its cranial end, impelling slosh away from the head.

On a modelling note, the simulations showed excellent agreement with the wavespeeds predicted by the analytical model of Cirovic (2009). With a syrinx, four waves were identified, which clearly corresponded to the waves predicted analytically. Without a syrinx, only three waves were found. The system as modelled seems then capable of supporting only three separate waves, even though four are predicted with the central canal reduced to microscopic size. Simulation of a system consisting of an ultra-long cord and dura, with continuous syrinx, allowed the explicit demonstration of the form of the waves that involve both cord and dura interacting, as well as those that are supported mainly in only one part of the overall structure.

The investigation also led to a greater understanding of the overall complexity of the wave propagation phenomena able to be supported by the system consisting of a syrinx-containing cord surrounded by CSF within the dura. Because all the models over-simplified the geometry of the SAS, wave attenuation was reduced. Conversely, reflections from the ends of the spinal SAS, particularly at the level of the base of the skull where the model terminated but the human does not, were increased. The anatomical transition from the spinal to the cranial SAS geometry will undoubtedly give rise to some reflection, but not as much as the abrupt cranial termination in the models. Furthermore, despite the introduction of filum-simulating structure in this model, the damping of waves remained small relative to that which seems to prevail in the real system. *In vivo*, the spindle-shaped caudal end of the SAS is expected to form rather an efficient wave absorber. For all of these reasons, reflections were more prominent in the models than in reality, and the opportunity thus presented was taken to examine the nature of refracted and reflected waves in detail. SAS pressure wave reflections certainly occur *in vivo*, as shown graphically by the resonant ringing recorded in conscious coughing humans by Williams (1976), even if their quantitative prevalence is at present uncertain. It is therefore important to include reflected waves in one's thinking about spinal cord system mechanics in general and syringomyelia in particular. However, as was emphasised previously (Bertram et al., 2005), the spinal cord system is short relative to the wavelengths created by most physiological excitation sources. Thus *in vivo*, although reflection, refraction and wave-splitting may be going on, it is expected that fewer waves will be separately discernible, and pressure variations will be closer to simultaneous and equal everywhere along the spinal cord system, except when events such as extremely percussive cough occur.

References

Berkouk, K., Carpenter, P.W., Lucey, A.D., 2003. Pressure wave propagation in fluid-filled co-axial elastic tubes, Part 1: basic theory. ASME Journal of Biomechanical Engineering 125, 852–856.

Bertram, C.D., Bilston, L.E., Stoodley, M.A., 2008. Tensile radial stress in the spinal cord related to arachnoiditis or tethering: a numerical model. Medical and Biological Engineering and Computing 46 (7), 701–707.

Bertram, C.D., Brodbelt, A.R., Stoodley, M.A., 2005. The origins of syringomyelia: numerical models of fluid/structure interactions in the spinal cord. ASME Journal of Biomechanical Engineering 127 (7), 1099–1109.

Brugières, P., Idy-Peretti, I., Iffenecker, C., Parker, F., Jolivet, O., Hurth, M., Gaston, A., Bittoun, J., 2000. CSF flow measurement in syringomyelia. American Journal of Neuroradiology 21 (10), 1785–1792.

Carpenter, P.W., Berkouk, K., Lucey, A.D., 2003. Pressure wave propagation in fluid-filled co-axial elastic tubes, Part 2: Mechanisms for the pathogenesis of syringomyelia. ASME Journal of Biomechanical Engineering 125, 857–863.

Chang, H.S., Nakagawa, H., 2003. Hypothesis on the pathophysiology of syringomyelia based on simulation of cerebrospinal fluid dynamics. Journal of Neurology, Neurosurgery and Psychiatry 74, 344–347.

Cirovic, S., 2009. A coaxial tube model of the cerebrospinal fluid pulse propagation in the spinal column. ASME Journal of Biomechanical Engineering 131, 021008.

Cirovic, S., Walsh, C., Fraser, W.D., 2002. Wave propagation in a system of coaxial tubes filled with incompressible media: a model of pulse transmission in the intracranial arteries. Journal of Fluids and Structures 16 (8), 1029–1049.

Crossman, A.R., Neary, D., 2005. Neuroanatomy: An Illustrated Colour Text, third ed. Elsevier Churchill Livingstone, Edinburgh.

Gardner, W.J., McMurry, F.G., 1976. "Non-communicating" syringomyelia: a non-existent entity. Surgical Neurology 6, 251–256.

Hall, P., Turner, M., Aichinger, S., Bendick, P., Campbell, R., 1980. Experimental syringomyelia: the relationship between intraventricular and intrasyrinx pressures. Journal of Neurosurgery 52 (6), 812–817.

Heiss, J.D., Patronas, N., DeVroom, H.L., Shawker, T., Ennis, R., Kammerer, W., Eidsath, A., Talbot, T., Morris, J., Eskioglu, E., Oldfield, E.H., 1999. Elucidating the pathophysiology of syringomyelia. Journal of Neurosurgery 91, 553–562.

Kalata, W., Martin, B.A., Oshinski, J.N., Jerosch-Herold, M., Royston, T.J., Loth, F., 2009. MR measurement of cerebrospinal fluid velocity wave speed in the spinal canal. IEEE Transactions on Biomedical Engineering 56 (6), 1765–1768.

Klekamp, J., 2002. The pathophysiology of syringomyelia—historical overview and current concept. Acta Neurochirurgica 144, 649–664.

Leyden, E., 1876. Ueber Hydromyelus und Syringomyelie. Archiv für pathologische Anatomie und Physiologie und für klinische Medicin 68 (1), 1–26.

Loth, F., Yardimci, M.A., Alperin, N., 2001. Hydrodynamic modelling of cerebrospinal fluid motion within the spinal cavity. ASME Journal of Biomechanical Engineering 123, 71–79.

Martin, B.A., Kalata, W., Loth, F., Royston, T.J., Oshinski, J.N., 2005. Syringomyelia hydrodynamics: an in vitro study based on in vivo measurements. ASME Journal of Biomechanical Engineering 127, 1110–1120.

Mazuchowski, E.L., Thibault, L.E., 2003. Biomechanical properties of the human spinal cord and pia mater. In: Proceedings of the ASME Summer Bioengineering Conference, Key Biscayne, Florida, pp. 1205–1206.

Milhorat, T.H., Capocelli, A.L., Kotzen, R.M., Bolognese, P., Heger, I.M., Cottrell, J.E., 1997. Intramedullary pressure in syringomyelia: clinical and pathophysiological correlates of syrinx distension. Neurosurgery 41 (5), 1102–1110.

Oldfield, E.H., Muraszko, K., Shawker, T.H., Patronas, N.J., 1994. Pathophysiology of syringomyelia associated with Chiari I malformation of the cerebellar tonsils. Journal of Neurosurgery 80, 3–15.

Ozawa, H., Matsumoto, T., Ohashi, T., Sato, M., Kokubun, S., 2001. Comparison of spinal cord gray matter and white matter softness: measurement by pipette aspiration method. Journal of Neurosurgery (Spine) 95, 221–224.

Ozawa, H., Matsumoto, T., Ohashi, T., Sato, M., Kokubun, S., 2004. Mechanical properties and function of the spinal pia mater. Journal of Neurosurgery (Spine) 1, 122–127.

Park, C.H., Chung, T.S., Kim, D.J., Suh, S.H., Chung, W.S., Cho, Y.E., 2008. Evaluation of intrasyrinx fluid motion by spatial modulation of magnetization-magnetic resonance imaging in syringomyelia with long-term follow-up: a predictor of postoperative prognosis? Journal of Computer Assisted Tomography 32 (1), 135–140.

Pinna, G., Alessandrini, F., Alfieri, A., Rossi, M., Bricolo, A., 2000. Cerebrospinal fluid flow dynamics study in Chiari I malformation: implications for syrinx formation. Neurosurgical Focus 8 (3), 1–8 Article 3.

Sakas, D.E., Korfias, S.I., Wayte, S.C., Beale, D.J., Papapetrou, K.P., Stranjalis, G.S., Whittaker, K.W., Whitwell, H.L., 2005. Chiari malformation: CSF flow dynamics in the craniocervical junction and syrinx. Acta Neurochirurgia (Wien) 147 (12), 1223–1233.

Sansur, C.A., Heiss, J.D., DeVroom, H.L., Eskioglu, E., Ennis, R., Oldfield, E.H., 2003. Pathophysiology of headache associated with cough in patients with Chiari I malformation. Journal of Neurosurgery 98 (3), 453–458.

Stockman, H.W., 2006. Effect of anatomical fine structure on the flow of cerebrospinal fluid in the spinal subarachnoid space. ASME Journal of Biomechanical Engineering 128 (1), 106–114.

The Visible Human Project®. US National Library of Medicine. 〈www.nlm.nih.gov/research/visible/visible_human.html〉.

Wilcox, R.K., Bilston, L.E., Barton, D.C., Hall, R.M., 2003. Mathematical model for the viscoelastic properties of dura mater. Journal of Orthopaedic Science 8, 432–434.

Williams, B., 1972. Combined cisternal and lumbar pressure recordings in the sitting position using differential manometry. Journal of Neurology, Neurosurgery and Psychiatry 35, 142–143.

Williams, B., 1976. Cerebrospinal fluid pressure changes in response to coughing. Brain 99, 331–346.

Williams, B., 1980. On the pathogenesis of syringomyelia: a review. Journal of the Royal Society of Medicine 73, 798–806.

Williams, B., 1986. Progress in syringomyelia. Neurological Research 8, 130–145.

Williams, B., 1990. Syringomyelia. Neurosurgery Clinics of North America 1 (3), 653–685.